Frequency-dependent source and load impedances in power systems based on power electronic converters

Atle Rygg
Marta Molinas
Department of Engineering Cybernetics
Norwegian University of Science and Technology
Trondheim, NORWAY
atle.rygg@itk.ntnu.no

Chen Zhang
Xu Cai
Department of State Energy Smart Grid R&D Center
Shanghai Jiao Tong University
Shanghai, CHINA
zhangchencumt@163.com

***Abstract*— Representations of power systems by frequency dependent impedance equivalents is an emerging technique in dynamic analyses of power systems including power electronic converters. The technique has been applied for decades in DC-power systems, and it has been recently adopted to map the impedances in AC systems. In the impedance-based stability analysis, the system is split into a source and load subsystem, both of which are represented by their respective frequency-dependent Norton and Thevenin equivalents. These equivalents can be obtained from analytic calculations, from numeric simulations, or from laboratory setup measurements. This paper will present a comparison of analysis and simulation-based techniques for obtaining the impedance equivalents. Different approaches for extraction of impedance equivalents are found in the literature but a rigorous comparison among the methodologies is still missing. Such comparison is relevant since non validated/verified impedance equivalents and extraction methods can lead to misleading conclusions. This work is attempting to bridge this gap by presenting a comparison of different simulation-based extraction methods and an analytical one.**

***Index Terms*—Grid impedance estimation, Power system stability, Power electronic systems, Frequency scanning**

I. INTRODUCTION

Analysis of power system dynamics and stability is challenging in systems with high penetration of power electronic converters. The combination of multiple nonlinearities and fast dynamics adds significant complexity to dynamic analysis. Impedance-based analysis of power systems can be a relevant and practical tool in this respect, as it reduces the system into a source and load subsystem, and analyses dynamic interactions between the two equivalents. [1][2].

This method has some highly appealing properties. First is the ability to consider the subsystems as "black-box", i.e. detailed knowledge of parameters and properties is not required as long as measurements can be applied at its terminals. Furthermore, the impedance equivalents can potentially be measured in a real system. The most accurate method for this purpose is based on frequency scanning [3][4]. The drawback of this method is the need for dedicated and complex equipment. Several alternative methods exist with ability to estimate impedance closer to real-time, and with low or zero additional hardware requirements. Examples are binary sequence injection [5], impulse response [6] and recurrent neural networks [7].

Once an impedance equivalent is established, it can be utilized for several purposes. Analytical impedance models for relatively simple systems were derived in [8][9][10], and the Generalized Nyquist Criterion (GNC) [11] was applied to evaluate the system stability. The impedance equivalents were also verified through experimental setups. This pure stability assessment is useful, but the utility improves if converter control systems can improve power system stability by adapting to changes in the grid. Utilizing impedance equivalents for this purpose was first performed in [12], and is often denoted *impedance shaping*. Similar approaches can be found in [13][14][15].

The previous works can be grouped into two directions. One is analyzing the system in the phase domain through symmetric components [1][5][6][9][13], while the other applies the synchronous (*dq*) reference frame [2][3][4][8][12]. Both domains have certain advantages and disadvantages, but neither a rigorous comparison nor an attempt to bridge them are conducted. Furthermore, both research directions suffer from the same challenge, namely how to verify the impedance equivalents. It is challenging to develop analytical models, and even more challenging to perform accurate measurements. Hence, thorough methodologies are required.

This paper is focusing how to obtain impedance equivalents by numeric simulations. Previous works applies different methods for this purpose, but a rigorous comparison between them is still missing. Detailed knowledge on these methods and their limitations and advantages is needed in order to have confidence in the results. Furthermore, establishing impedance equivalents by simulations is an

important step towards experimental setups in laboratories or full-scale systems. The paper outline is as follows: Section II describes the applied methods for obtaining impedance equivalents through custom-built routines in Matlab. Section III presents the case study system being analyzed, while section IV outlines the derivation of an analytical impedance model for the same system. Section V contains the results, while recommendations and conclusions are presented in sections VI and VII.

II. Obtaining impedance equivalents by simulation

When the impedance equivalents are obtained through numeric simulations, a disturbance, or perturbation, is injected at the defined interface point between source and load subsystems, see Figure 1. The disturbance is normally selected either as a shunt current injection, or as a series voltage injection. The applicability of injection method depends on the ratio between source and load impedance at a given frequency. The system with lowest impedance is suited for current injection, since it will absorb most of the injected current. However, the opposite conclusion holds for series voltage injection. In other words, it can be difficult to estimate both impedances using one of the methods.

The second choice is related with frequency content. The perturbation can contain a sum of several frequency components (*multi-tone*), or each frequency can be injected individually (*single-tone*). The single-tone approach is also denoted frequency scanning/sweeping, and is expected to be more accurate. However, as multi-tone requires only a single injection signal, the required simulation time is significantly lower, and processing is faster. This is also advantageous in experimental setups, as the method is more close to real-time. Additionally, the multi-tone principle is not limited to sinusoidal signals. Binary signal injection is performed in [5], while impulse-response is conducted in [6]. It is remarked that a challenge associated with multi-tone injection is the possible cross-coupling between different frequency. This was investigated in [16] in the case of diode rectifier loads.

A. Challenges

There are two main challenges that complicates the task of estimating frequency dependent impedance equivalents of AC power systems with high power electronics penetration. First, the impact of power electronics and control non-linearities. The impedances are generally dependent on the actual operation point of the system, and must hence be evaluated in a neighborhood of this point. For analytical impedance calculations, this is handled through linearization and small-signal analysis. For simulation or measurement-based analysis, a small disturbance is superimposed into the system during operation, and the results must be accurately processed to obtain the impedance equivalents. The second challenge is the lack of a well-defined equilibrium point in three-phase AC-systems' time varying instantaneous voltage and currents. The impedance approach performs a linearization around a steady-state equilibrium, and this is not straightforward when the system instantaneous voltages and currents are alternating. This challenge is addressed by introducing sequence domain decomposition [1] or synchronous reference frame transformation [2] to obtain an equilibrium point where all state variables are constant.

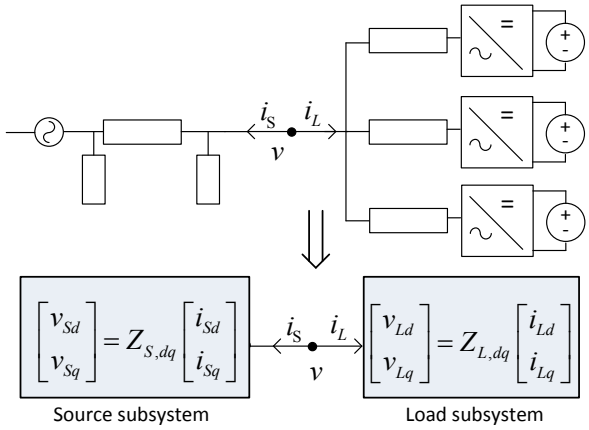

Figure 1: Illustration of impedance-based dynamic modeling of power system in *dq*-domain

B. Outline of procedure

The synchronous (*dq*)-reference frame is applied in this work, but the methodology is very similar for the sequence domain. The following section presents the procedure applied to obtain the impedance equivalents, referring to the flowcharts in Figure 2. The procedure are identical for both series voltage and shunt current injection. On the other hand, there are minor differences between single-tone injection and multi-tone injection as seen in the figure. Still, the following main principles remain the same:

1) Frequency selection
2) Simulation
3) FFT and related calculations
4) Impedance calculation

Each of these steps are now described in detail, using the following nomenclature:

- lower case: time-domain signals
- UPPER case: Frequency domain signals (complex)
- **BOLD** upper case: Vectors of complex numbers
- **<u>BOLD</u>** underlined upper case: Matrix of vectors of complex numbers, typically a *2x2* matrix

1) Frequency selection

The first step is to select a vector of frequencies $f_{tab} = [f_1, f_2, ..., f_n]$ where the impedance should be estimated. The vector can normally be chosen arbitrarily, but the fundamental (e.g. 50 Hz) should be omitted since the presence of background voltages and currents will corrupt the impedance calculation at this frequency unless dedicated techniques are applied to remove these components.

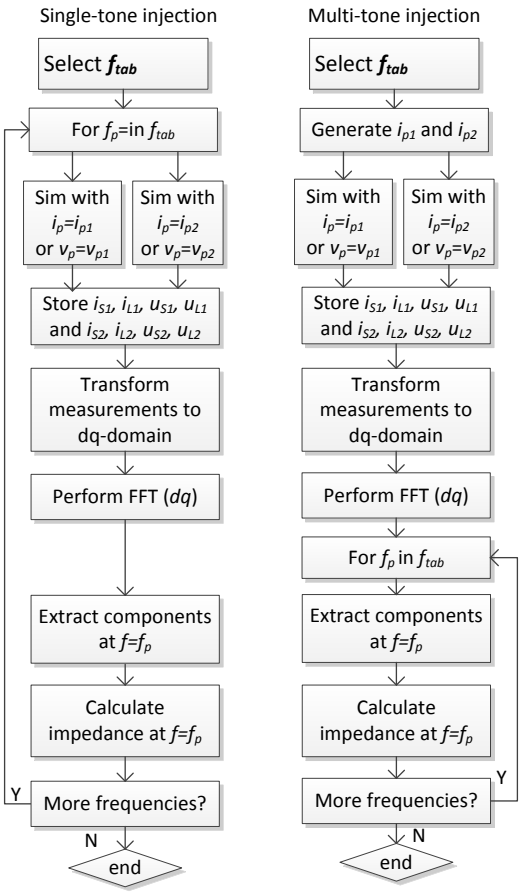

Figure 2: Flowchart for impedance estimation by simulation in dq-domain. Left: Single-tone, right: Multi-tone

2) Simulation

The next step is to simulate the system with proper perturbation injection applied. Since there are four impedances to be estimated, at least two sets of linear independent perturbation signals need to be applied separately [2][3]. These are denoted i_{p1}, i_{p2} for shunt current injection, and u_{p1}, u_{p2} for series voltage injection. They can be generated in many ways, and in this paper, the following choice is made:

- First perturbation (i_{p1} or u_{p1}): Symmetrical three-phase positive sequence perturbation
- Second perturbation (i_{p2} or u_{p2}): Symmetrical three-phase negative sequence perturbation

Since the frequencies in f_{tab} are referred to the *dq*-frame, the perturbation must be transformed back to phase domain in order to be compatible with the injection structure in Figure 3. The following phase-domain equations will give the desired frequency component in the *dq*-domain:

$$i_{p1}^{abc} = I_{p1,mag}\begin{bmatrix} \sin\left(\left(\omega_p+\omega_1\right)t+\varphi_{p1}\right) \\ \sin\left(\left(\omega_p+\omega_1\right)t-\frac{2\pi}{3}+\varphi_{p1}\right) \\ \sin\left(\left(\omega_p+\omega_1\right)t+\frac{2\pi}{3}+\varphi_{p1}\right) \end{bmatrix} \quad (1)$$

$$i_{p2}^{abc} = I_{p2,mag}\begin{bmatrix} \sin\left(\left(\omega_p-\omega_1\right)t+\varphi_{p2}\right) \\ \sin\left(\left(\omega_p-\omega_1\right)t+\frac{2\pi}{3}+\varphi_{p2}\right) \\ \sin\left(\left(\omega_p-\omega_1\right)t-\frac{2\pi}{3}+\varphi_{p2}\right) \end{bmatrix} \quad (2)$$

where ω_1 is the fundamental frequency of the system, ω_p is the perturbation frequency, $I_{p,mag}$ is the magnitude of perturbation, while φ_p is the perturbation phase angle. The choice of perturbation magnitude is discussed later, while the phase angle can be chosen arbitrarily. Note that corresponding equations can be obtained for series voltage injection by simply replacing *"i"* with *"u"*. The relevant measurements to store are the three-phase time-domain source current and voltage i_S^{abc}, u_S^{abc} and the load current and voltage i_L^{abc}, u_L^{abc}, see Figure 1. For single-tone injection, equations (1) and (2) are applied directly in individual simulations for each element in f_{tab}. For multi-tone injection, the different frequency components are combined into a combined perturbation signal as follows:

$$i_{p1,Mu}^{abc} = \sum_{i=1}^{n} i_{p1}^{abc}\left(\omega_i, \varphi_{p,i}\right) \quad (3)$$

Where i_{p1}^{abc} is the single-tone three-phase signal from (1).

3) FFT and related calculations

In this paper, the impedances are calculated in the synchronous (*dq*) reference frame. Hence, the measured time-domain phase signals must be transformed to the *dq* frame. This is achieved through the Parks Transform. The synchronous reference frame time-domain vectors can directly be transformed into the frequency domain by a Fast Fourier Transform (FFT) algorithm. With the d-axis voltage as an example, the desired output from the FFT-calculation is a vector of complex numbers $\boldsymbol{U_d} = \left[U_{d,1}, U_{d,2}, ..., U_{d,N}\right]$ that will reproduce the time-domain vector u_d as follows:

$$u_d\left(t_i\right) = \sum_{j=1}^{N} \left|U_{d,j}\right| \sin\left(\omega_k t_i + \angle U_{d,j}\right) \quad (4)$$

$t_i = t_0 + i \cdot \Delta t$ is a discrete time instant from the simulation results, assuming a fixed-step solver with time step Δt. N is the number of data points in the time-series, which also equals the number of elements in $\boldsymbol{U_d}$. Similarly, ω_k is the

frequency corresponding to the k^{th} element of $\boldsymbol{U}_d$, and can be written as $\omega_k = 2\pi \frac{k-1}{T_{fft}}$, where $T_{fft} = N\Delta t$ is the total duration of the time-domain input to the FFT.

With single-tone injection, only one element in $\boldsymbol{U}_d$ is of interest per simulation, namely the element with index k such that $\omega_k = \omega_p$, i.e. the perturbation frequency from (1). According to the flowchart in Figure 2, this element is then extracted for all relevant voltage and current measurements. The same procedure must then be repeated n times, once for each element in f_{tab}.

With multi-tone injection, all frequencies are incorporated into a combined perturbation signal. Hence, the FFT needs only to be performed once, and all relevant elements can be extracted from the same FFT-vector. This will again yield n elements, one per frequency in f_{tab}. This is also illustrated in Figure 2.

4) Impedance calculation

The final step is to calculate the impedances based on the set of complex dq-domain voltage and current vectors. This is achieved by solving the following matrix for $\underline{\boldsymbol{Z}}_{dq}$:

$$\begin{bmatrix} \boldsymbol{U}_{d1} & \boldsymbol{U}_{q1} \\ \boldsymbol{U}_{d2} & \boldsymbol{U}_{q2} \end{bmatrix} = \overbrace{\begin{bmatrix} \boldsymbol{Z}_{dd} & \boldsymbol{Z}_{dq} \\ \boldsymbol{Z}_{qd} & \boldsymbol{Z}_{qq} \end{bmatrix}} \cdot \begin{bmatrix} \boldsymbol{I}_{d1} & \boldsymbol{I}_{q1} \\ \boldsymbol{I}_{d2} & \boldsymbol{I}_{q2} \end{bmatrix} \quad (5)$$

Recall that the notation implies that this is a matrix equation of complex vectors, e.g. $\boldsymbol{U}_{d1} = \left[U_{d1,1}, U_{d1,2}, ..., U_{d1,n}\right]$ etc., hence the impedance matrix needs to be solved n times, once for each perturbation frequency in f_{tab}.

III. CASE STUDY SYSTEM

A simple benchmark system is developed and implemented for the analysis, and is presented in Figure 3. The system contains a single grid-connected Voltage Source Converter (VSC), including its filter impedance Z_{conv}. The grid is modeled with equivalent Thevenin voltage v_{th} and impedance Z_{th}.

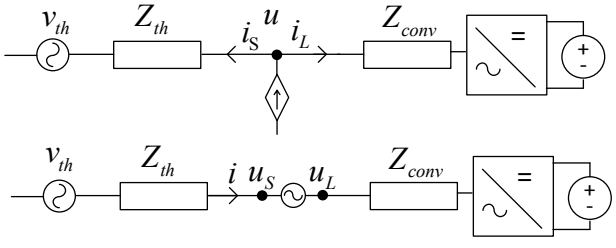

Figure 3: Benchmark system containing a single grid-connected converter. Upper figure: shunt current injection. Lower figure: series voltage injection.

The key part of the case study system is the VSC control system. Although control systems do not represent an impedance under the traditional definition, it will be shown later that it contributes to altered input impedance of the VSC. This additional impedance is highly dependent on the operation point as well as the frequency, and is difficult to obtain from calculations unless all parameter values are known with high accuracy.

The control system applied in the analysis is a current control scheme in the synchronous (dq) reference frame, including decoupling and feed-forward terms. See Figure 5 for an overview. K_{pi} and T_{ii} are the current PI controller gain and integration time constant, respectively. T_u is the filter time constant for the voltage feed-forward. ω_1 is the fundamental frequency in rad/s, while θ_{PLL} is the fundamental phase angle obtained from the Phase Lock Loop (PLL). A standard Pulse-Width Modulation (PWM) scheme is applied to obtain the resulting gate signal commands g1…g6 in the two-level VSC.

The PLL has also significant impact on the resulting converter impedance. Hence, both the choice of PLL structure and its tuning is important. In this work, a standard Synchronous Reference Frame PLL (SRF-PLL) is applied, see Figure 4. The voltage measurement is applied on the grid side of the filter Z_{conv}, and is normalized to obtain per unit values. K_{PLL} is the controller gain.

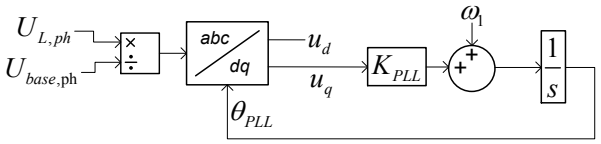

Figure 4: Structure of Synchronous Reference Frame Phase Lock Loop (SRF-PLL)

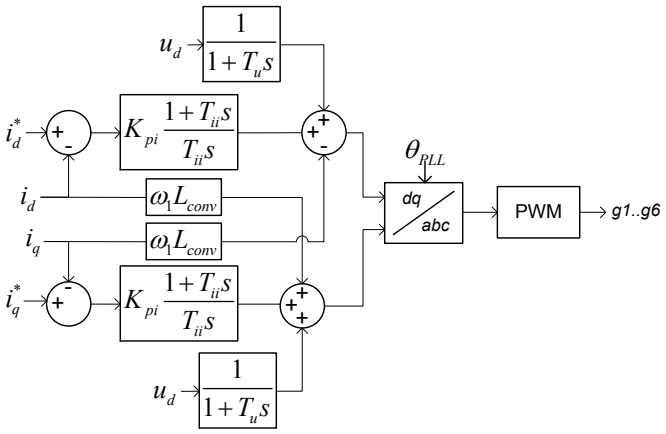

Figure 5: Structure of VSC control system with synchronous reference frame current control

IV. VSC ANALYTICAL IMPEDANCE MODEL

Previous works have contributed to development of VSC impedance models in the synchronous reference frame. For details on how such models can be derived, see [8]. It is also possible to derive models directly in the phase domain as shown in [9]. The procedure of deriving impedance models is based on small-signal analysis. Non-linear parts of the system need to be linearized around a stationary point. Two nonlinearities are considered in the converter model applied in this work:

- *abc-to-dq* transformation in the PLL
- Pulse-Width Modulation and sampling delay

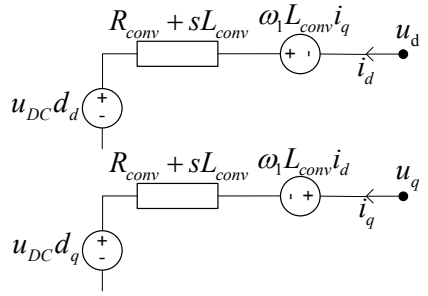

Figure 6: VSC equivalent in the synchronous reference frame

The model is based on the converter equivalent in the synchronous reference frame as presented in Figure 6. The objective is to express all state variables in the system as a linear function of i_d, i_q, u_d, u_q and to rearrange/solve these expressions to comply with the following notation:

$$\underline{u}_{dq} = \begin{bmatrix} u_d \\ u_q \end{bmatrix} = \begin{bmatrix} Z_{dd} & Z_{dq} \\ Z_{qd} & Z_{qq} \end{bmatrix} \begin{bmatrix} i_d \\ i_q \end{bmatrix} = \underline{Z}_{dq} \underline{i}_{dq} \tag{6}$$

The main challenge in this procedure is to handle the terms $u_{DC} d_d$ and $u_{DC} d_q$ properly. In this work a constant DC-voltage is assumed, hence it is sufficient to express the duty cycles as a function of i_d, i_q, u_d, u_q. However, due to the dynamics of the PLL, an angular shift between the system reference frame and the control system reference frame is introduced. By linearizing the angular shift or error can be estimated as [8]:

$$\Delta\theta = \theta^c_{PLL} - \theta^s_{PLL} = \overbrace{\frac{H_{PLL}(s)}{s + H_{PLL}(s) V^s_d}} \Delta u^s_q = G_{PLL} \Delta u^s_q \tag{7}$$

Where superscript *'s'* denotes the system reference frame, while *'c'* denotes the converter reference frame as defined in [8]. $H_{PLL} = K_{PLL}$ is the PLL transfer function, while Δu^s_q denotes the small-signal value of the q-axis voltage in the connection point. With this estimate of $\Delta\theta$ the control system can be referred to the system domain by appropriate transformation matrices. Mathematical details are omitted here since the development is based on [8].

The resulting impedance model can be written as

$$Z_{dq} = \left(I - U_{DC} \left(G_{cc} G_{pwm} G^i_{PLL} + G_{fv} G_{pwm} G^v_{PLL} + G^d_{PLL} \right) \right)^{-1} \cdot \left(Z_0 + U_{DC} G_{cc} G_{pwm} \right) \tag{8}$$

where I is the *2x2* identity matrix, U_{DC} is the constant DC-voltage, and the transfer functions given by:

$$G_{cc} = \begin{bmatrix} K_{pi} \dfrac{1 + T_{ii} s}{T_{ii} s} & 0 \\ 0 & K_{pi} \dfrac{1 + T_{ii} s}{T_{ii} s} \end{bmatrix}$$ - Current controller

$$G_{PWM} = \begin{bmatrix} H_{PWM} & 0 \\ 0 & H_{PWM} \end{bmatrix}$$ - PWM delay approximation

$$G_{fv} = \begin{bmatrix} \dfrac{1}{1 + T_u s} & 0 \\ 0 & \dfrac{1}{1 + T_u s} \end{bmatrix}$$ - Voltage feed-forward filter

$$G^i_{PLL} = \begin{bmatrix} 0 & G_{PLL} I^s_q \\ 0 & -G_{PLL} I^s_d \end{bmatrix}$$ - Current PLL shift

$$G^d_{PLL} = \begin{bmatrix} 0 & -G_{PLL} D^s_q \\ 0 & G_{PLL} D^s_d \end{bmatrix}$$ - Duty cycle PLL shift

$$G^d_{PLL} = \begin{bmatrix} 1 & G_{PLL} V^s_d \\ 0 & 1 - G_{PLL} V^s_d \end{bmatrix}$$ - Voltage PLL shift

$$Z_0 = \begin{bmatrix} R_{conv} + sL_{conv} & -\omega_1 L_{conv} \\ \omega_1 L_{conv} & R_{conv} + sL_{conv} \end{bmatrix}$$ - Filter impedance

The parameters $I^s_q, I^s_d, D^s_d, D^s_q, V^s_d, V^s_q$ represent the steady-state operation point for current, duty cycle and voltage, and must be obtained from either analytic calculation or from numeric simulation. It is remarked that although the reference system contains only a single converter, the resulting analytic impedance model is complicated to derive. For larger systems containing many converters, transformers, lines and cables, development of analytical impedance models seems not a practical approach. However, they are useful for comparison purposes in the simple system analyzed in this paper, as will be shown in the next section.

V. RESULTS

The results presented in this section are all based on the system in Figure 3, with the operating point and parameter values given in Table 1. The operation point is arbitrarily chosen, and represents a condition with a relatively highly loaded converter. Due to space limitations, the comparison is presented for the load impedance equivalent only. This is also

justified from the fact that the source subsystem is limited to a Thevenin equivalent. The impedance is simulated and compared for nine cases, see Table 2

Figure 7 and Figure 8 show the comparison between average model cases (1 to 4) and switching model cases (5 to 8), respectively. The analytical model (case 0) is included in both figures. The average model cases have close to equal impedance in all channels for all frequencies. The match with the analytical model is also good. Some deviations with the analytic model can be seen at the highest frequencies. This is expected to be caused by the non-linear behavior of the PWM. In addition, there is some mismatch for the impedance Z_{qd}. This is explained by the fact that its value is 1-2 decades lower than the other, and is hence very challenging to estimate.

The switching model results presented in Figure 8 are not as accurate as the average model results. The match is relatively good for the diagonal elements Z_{dd} and Z_{qq}, while the off-diagonal elements Z_{dq} and Z_{qd} are significantly corrupted by noise. Apparently, the two methods based on series voltage injection performs better than shunt current injection. The latter phenomena is expected since a current controlled converter is high-ohmic, and consequently the grid will absorb most of the injected current.

Table 1: Case study information and parameters

Parameter	Value	Parameter	Value
Grid voltage	690 V	**d-axis current**	0.8 p.u.
System power base	1 MVA	**q-axis current**	0.5 p.u. cap.
Grid impedance	0.01+j0.15 p.u.	**Converter DC-voltage**	1400 V
Filter impedance	0.01+ j0.15 p.u.	**Converter switching frequency**	2500 Hz
Converter type	2-level	**Converter filter type**	L
Converter modulation	Sinusoidal PWM		

Table 2: Overview of cases

Case nr.	Series voltage/ Shunt current	Single-tone/ Multi-tone	Average model/ Switching model
Case 0	*Analytical model*		
Case 1	Voltage	Single	Average
Case 2	Current	Single	Average
Case 3	Voltage	Multi	Average
Case 4	Current	Multi	Average
Case 5	Voltage	Single	Switching
Case 6	Current	Single	Switching
Case 7	Voltage	Multi	Switching
Case 8	Current	Multi	Switching

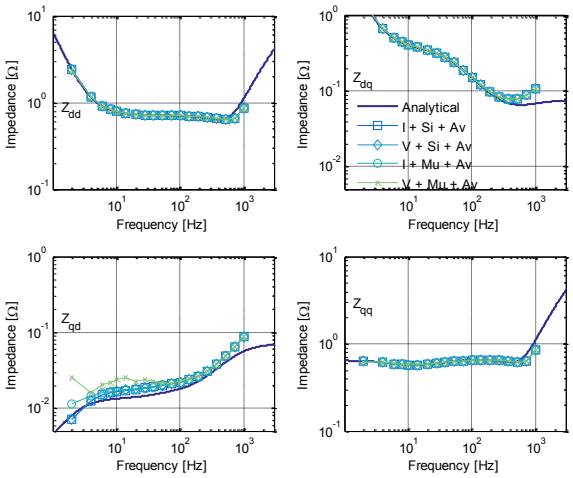

Figure 7: Comparing analytical model (Case 0) with average model cases (1 to 4)

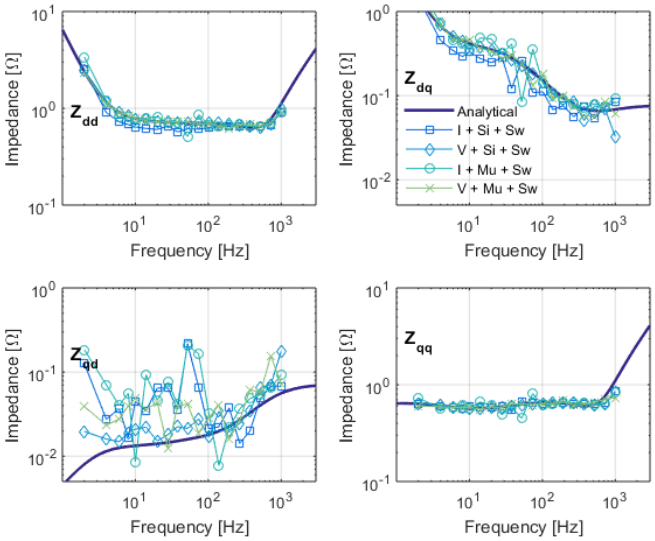

Figure 8: Comparing analytical model (case 0) with switching model cases (5 to 8)

The ability to estimate accurately the impedance equivalents depends also on the magnitude of perturbation injection. This is equivalent to the value of $I_{p,mag}$ in (1). A too high value can have impact on the operation point, hence making the small-signal assumption invalid. On the other hand, a too low value introduces challenges with signal processing and numeric accuracy. Based on these issues, a sensitivity analysis is conducted for two of the eight simulation-based methods, both based on series voltage injection and single-tone injection. Figure 9 shows the result for Case 1 (V+Si+Av), while Figure 10 shows the results for Case 5 (V+Si+Sw). With average model, the perturbation magnitude can be reduced to 0.05 % without any visible impact on the impedance equivalent. However, for the largest perturbation magnitude (20 %), the impedance is affected due to a violated small-signal assumption.

With switching model in Figure 10, a similar impact is present for the highest value of perturbation (20 %), although the error is larger. Additionally, the lowest value (0.05 %) is corrupted by noise.

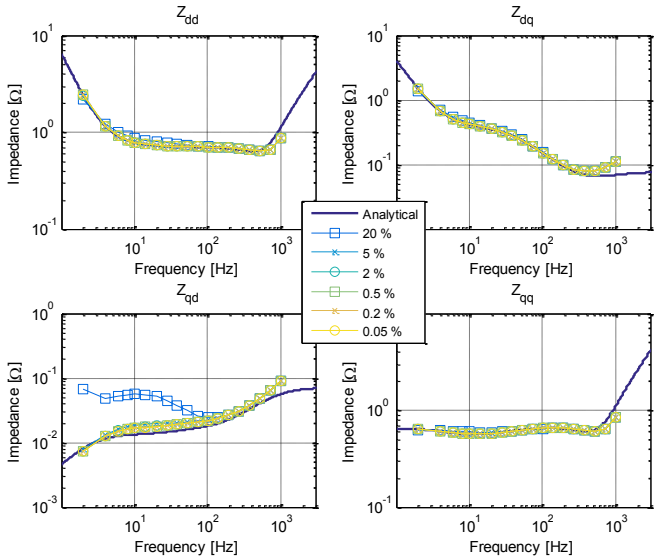

Figure 9: Sensitivity to perturbation magnitude for Case 1 (V + Si + Av). Perturbation current measured in percent of nominal converter current.

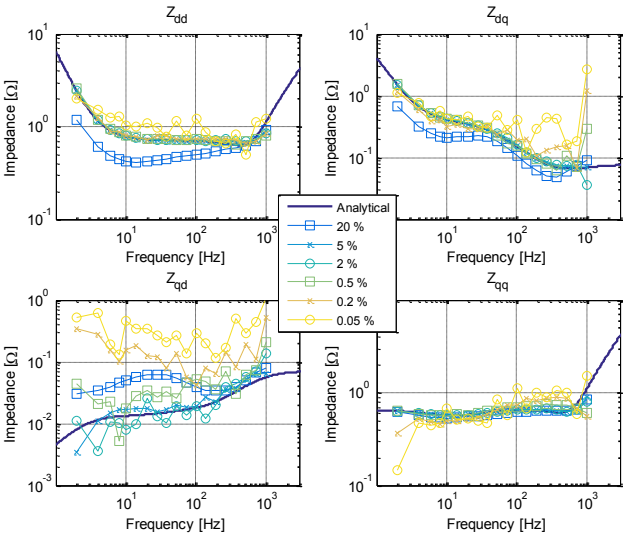

Figure 10: Sensitivity to perturbation magnitude for Case 5 (V+Si+Sw). Perturbation current measured in percent of nominal converter current.

VI. Recommendations

In this paper, nine methods for impedance extraction are compared for a given case study system. When choosing method, one must be aware of the trade-off between accuracy and computational demand. It is evident that the switching models are most accurate, but they bring a significant increase in simulation time. In addition, switching noise and harmonics can corrupt the impedance estimates as explained before. Furthermore, since the systems under study are normally more complex than in Figure 3, switching models are in many cases unpractical. The recommendation is therefore to apply average models for converters, but to represent the switching delay and PWM with sufficient accuracy.

The choice between single-tone and multi-tone is also a trade-off between accuracy and computational demand. Single-tone is expected to be more robust and accurate, but can take significantly longer simulation time.

When choosing between shunt and series injection, one must identify the subsystem with most complex impedance behavior. If this is the high-ohmic subsystem, series injection is preferred. Otherwise, shunt injection is preferred. Note that this choice is related with numeric accuracy and robustness, and both methods are in principle able to find equal models.

VII. Conclusions

This paper has investigated several methods for obtaining frequency dependent impedance equivalents of power systems based on power electronic converters. Such impedance equivalents can be applied in stability and harmonic analysis of complex systems. They can be extracted from analytic calculations, from numeric simulations, or from experimental setups. The possibility to on-line estimate impedance equivalents is an appealing property with great potential for further research.

The paper has compared nine methods for impedance extraction in a reference system including a single grid-connected voltage source converter. One method is based on an analytical model, while the remaining eight are simulation-based. The methods are composed by combinations of

- Series voltage vs. shunt current injection
- Single-tone vs. multi-tone injection
- Average model vs. switching converter model

The match between the analytical model and the simulation results are in general good. Consequently, when analytical models are available they can be used for stability analysis without performing any simulation. The advantage of this is the short calculation time needed to obtain the impedances. The drawback is the challenge in obtaining the model for a large system with multiple units. In addition, it can be challenging to linearize accurately the model around the relevant operation point.

Generally, the results confirm that all nine methods are able to estimate the same impedance equivalent, assuming a proper choice of perturbation magnitude. The most challenging methods are the combinations of switching model and shunt current injection. The high frequency components introduced by the converter switches partly corrupts the

impedance extraction, and further work should find methods to handle this noise. Furthermore, the methods based on shunt-current injections performs slightly worse than those based on series-voltage injection. However, this is not a general rule, and depends on which of the subsystems (source or load) that has the largest impedance at a given frequency.

REFERENCES

[1] Jian Sun, "Small-Signal Methods for AC Distributed Power Systems–A Review," *Power Electronics, IEEE Transactions on* , vol.24, no.11, pp.2545,2554, Nov. 2009

[2] Belkhayat, M.; "Stability criteria for AC power systems with regulated loads", PhD-thesis, Purdue University, 1997

[3] Francis, G.; Burgos, R.; Boroyevich, D.; Wang, F.; Karimi, K., "An algorithm and implementation system for measuring impedance in the D-Q domain, *"Energy Conversion Congress and Exposition (ECCE),* 2011 IEEE , vol., no., pp.3221,3228, 17-22 Sept. 2011

[4] Familiant, Y.A.; Jing Huang; Corzine, K.A.; Belkhayat, M., "New Techniques for Measuring Impedance Characteristics of Three-Phase AC Power Systems*," Power Electronics, IEEE Transactions on* , vol.24, no.7, pp.1802,1810, July 2009

[5] Roinila, T.; Vilkko, M.; Jian Sun, "Online Grid Impedance Measurement Using Discrete-Interval Binary Sequence Injection*," Emerging and Selected Topics in Power Electronics, IEEE Journal of* , vol.2, no.4, pp.985,993, Dec. 2014

[6] Cespedes, M.; Jian Sun, "Adaptive Control of Grid-Connected Inverters Based on Online Grid Impedance Measurements*," Sustainable Energy, IEEE Transactions on* , vol.5, no.2, pp.516,523, April 2014

[7] Peng Xiao; Venayagamoorthy, G.K.; Corzine, K.A.; Jing Huang, "Recurrent Neural Networks Based Impedance Measurement Technique for Power Electronic Systems," *Power Electronics, IEEE Transactions on* , vol.25, no.2, pp.382,390, Feb. 2010

[8] Wen, B.; Dong, D.; Boroyevich, D.; Burgos, R.; Mattavelli, P.; Shen, Z., "Impedance-Based Analysis of Grid-Synchronization Stability for Three-Phase Paralleled Converters," *Power Electronics, IEEE Transactions on* , vol.PP, no.99, pp.1,1

[9] Cespedes, M.; Jian Sun, "Impedance Modeling and Analysis of Grid-Connected Voltage-Source Converters," *Power Electronics, IEEE Transactions on* , vol.29, no.3, pp.1254,1261, March 2014

[10] Xiongfei Wang; Blaabjerg, F.; Weimin Wu, "Modeling and Analysis of Harmonic Stability in an AC Power-Electronics-Based Power System*," Power Electronics, IEEE Transactions on* , vol.29, no.12, pp.6421,6432, Dec. 2014

[11] Desoer, C.A.; Yung-Terng Wang, "On the generalized nyquist stability criterion," *Automatic Control, IEEE Transactions on* , vol.25, no.2, pp.187,196, Apr 1980

[12] Harnefors, Lennart; Bongiorno, M.; Lundberg, S., "Input-Admittance Calculation and Shaping for Controlled Voltage-Source Converters," *Industrial Electronics, IEEE Transactions on* , vol.54, no.6, pp.3323,3334, Dec. 2007

[13] Cespedes, M.; Jian Sun, "Impedance shaping of three-phase grid-parallel voltage-source converters," *Applied Power Electronics Conference and Exposition (APEC), 2012 Twenty-Seventh Annual IEEE* , vol., no., pp.754,760, 5-9 Feb. 2012

[14] Radwan, A.A.A.; Mohamed, Y.A.-R.I., "Analysis and Active-Impedance-Based Stabilization of Voltage-Source-Rectifier Loads in Grid-Connected and Isolated Microgrid Applications," *Sustainable Energy, IEEE Transactions on* , vol.4, no.3, pp.563,576, July 2013

[15] Alawasa, K.M.; Mohamed, Y.A.-R.I.; Xu, W., "Active Mitigation of Subsynchronous Interactions Between PWM Voltage-Source Converters and Power Networks,"*Power Electronics, IEEE Transactions on* , vol.29, no.1, pp.121,134, Jan. 2014

[16] Bo Zhou; Jaksic, M.; Zhiyu Shen; Bo Wen; Mattavelli, P.; Boroyevich, D.; Burgos, R., "Small-signal impedance identification of three-phase diode rectifier with multi-tone injection," *Applied Power Electronics Conference and Exposition (APEC), 2014 Twenty-Ninth Annual IEEE* , vol., no., pp.2746,2753, 16-20 March 2014